Fuel 198 (2017) 3–10

Contents lists available at ScienceDirect

Fuel

journal homepage: www.elsevier.com/locate/fuel

Full Length Article

Photodegradation of pharmaceutical drugs using Sn-modified TiO_2 powders under visible light irradiation

D.A. Solís-Casados [a,c,*], L. Escobar-Alarcón [b], L.M. Gómez-Oliván [c], E. Haro-Poniatowski [d], T. Klimova [e]

[a] Centro Conjunto de Investigación en Química Sustentable UAEM-UNAM, Km 14.5 Carretera Toluca-Atlacomulco, Unidad San Cayetano, Toluca, Estado de México C.P. 50200, México
[b] Departamento de Física, Instituto Nacional de Investigaciones Nucleares, Apdo. Postal 18-1027, México, D.F. C.P. 11801, México
[c] Facultad de Química, Universidad Autónoma del Estado de México, Paseo Colon esq Paseo Tollocan Col Nueva la Moderna, Toluca, Estado de México C.P. 50 000, México
[d] Departamento de Física, Universidad Autónoma Metropolitana Iztapalapa, Apdo. Postal 55-534, México, D.F., México
[e] Departamento de Ingeniería Química, Facultad de Química, Universidad Nacional Autónoma de México (UNAM), Cd. Universitaria, Coyoacán, 04510 Ciudad de México, México

HIGHLIGHTS

- Sn incorporation into the TiO_2 lattice can tailor the anatase to rutile ratio.
- Sn-modified TiO_2 photocatalyst remove selectively different NSAIDs.
- NSAIDs degradation present in real wastewaters was achieved.

GRAPHICAL ABSTRACT

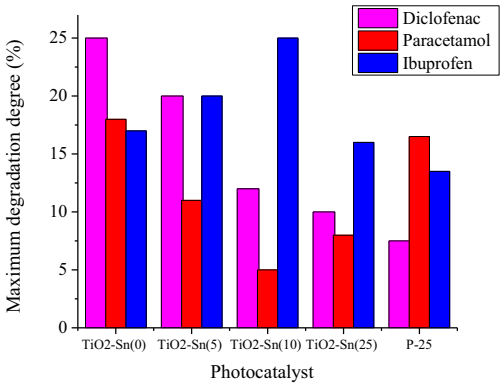

ARTICLE INFO

Article history:
Received 15 May 2016
Received in revised form 12 January 2017
Accepted 14 January 2017
Available online 21 January 2017

Keywords:
Photocatalysis
Anatase
Rutile
NSAIDs
Wastewaters

ABSTRACT

Sn-modified TiO_2 powders with different amounts of tin (0, 2.4, 5.1 and 7.2 at.%) were obtained by the surfactant-assisted technique using Pluronic P123 as template. The synthesis procedure favors the formation of a mixture anatase/rutile at annealing temperatures as low as 350 °C. The incorporation and further increase of the tin content promotes the transformation of anatase to rutile phase allowing to vary the anatase to rutile ratio in a controlled way, reaching the rutile phase the 96% of the mixture at a Sn content of 7.2 at.%. The synthesized materials were tested in the photocatalytic degradation of the NSAIDs, diclofenac, ibuprofen and paracetamol present in real wastewaters to evaluate their catalytic performance under visible light. The obtained results seem to indicate a certain kind of selectivity or affinity for degradation of each specific drug with a catalyst.

1. Introduction

In recent years, wastewaters from domestic and industrial uses have created a major environmental problem because these are generally released into the soil and aquifers with the consequent pollution of water. Among the pollutants in wastewaters are organic compounds such as phenols, dyes, pesticides, drugs, sol-

* Corresponding author at: Centro Conjunto de Investigación en Química Sustentable UAEM-UNAM, Km 14.5 Carretera Toluca-Atlacomulco, Unidad San Cayetano, Toluca, Estado de México C.P. 50200, México.
E-mail address: solis_casados@yahoo.com.mx (D.A. Solís-Casados).

http://dx.doi.org/10.1016/j.fuel.2017.01.059
0016-2361/

vents and fertilizers. Most of these compounds are toxic to humans and other living organisms, especially the aquatic life, even when they are present in low concentrations [1–3]. Specifically, the Non-Steroidal anti-Inflammatory Drugs (NSAID) have attracted special attention because of their resilience and stable chemical structure that once are introduced to the environment become in refractory pollutants. It is well known that NSAIDs can come from hospital effluents as well as from pharmaceutical industry; it is worth noting that domestic effluents can also contain quantities of pharmaceuticals since they can be acquired without medical prescription and are excreted in a high percentage with the urine [4,5]. Then, water polluted with NSAIDs has attracted the interest of researchers from different scientific disciplines around the world and, in this particular case of study, the water used from different effluents of a pharmaceutical industry in the State of Mexico, containing separately paracetamol, ibuprofen and diclofenac. Several solutions have been proposed in order to diminish or eliminate the amount of organic pollutants contained in wastewaters, and even to improve its quality, focused on the use of advanced oxidation processes (AOPs). Among the most studied are the photocatalytic processes where a semiconductor material is used for the removal, degradation and mineralization of organic molecules present in aqueous systems. In this process the catalyst is activated using electromagnetic radiation becoming a good alternative for environmental remediation [6,7]. It is noteworthy that the process of degradation of organic compounds dissolved in water occurs under the irradiation of sunlight in a natural way; however, this has a very low efficiency since the organic compounds degrade slowly, taking sometimes several days to achieve the complete mineralization (transformation of organic compounds to CO_2 and water) [8,9]. In order to enhance the degradation rate, the design of more efficient photocatalysts remains as an important issue. The most widely employed photocatalyst has been TiO_2, in the anatase phase mainly, because of its capability to oxidize organic compounds dissolved in water, non-toxicity, low-cost and its long-term photostability [10]. This photocatalyst can carry out the degradation of up to 75% of some organic compounds over periods of 3–4 h. However, TiO_2 has an important drawback owing to its relatively high band gap, close to 3.2 eV for the anatase phase. This implies that TiO_2 can only be activated with wavelengths lower than 387 nm, i.e. with ultraviolet light [11]. It has been found that the anatase phase primarily shows higher activity under UV irradiation, whereas the mixtures of anatase–rutile crystalline phases have been reported to show photoactivity at higher wavelengths, in the visible region, which can be attributed to a narrow band gap of these mixtures. Therefore, the high value of the TiO_2 band gap energy limits its application using solar light because 90% of the solar radiation reaching the earth's surface has wavelengths greater than 427 nm [12,13]. In order to improve the photocatalytic performance of TiO_2 under visible light, the TiO_2 doping with metals (Ni, Co, Zn, Fe, Ag, Cu W, Nb, Pd, Sn, Sb or Bi) [14–16], non-metals (N, S or C) [17,18] and the coupling with another semiconductor with wider or narrow band gap energy (SiO_2, ZrO_2, Al_2O_3, SnO_2, WO_3, ZnO, CeO_2) have been investigated [19,20]. It has been found that some metals and non-metals can narrow the band gap energy to sensitize catalysts under visible light, however the recombination rate of the electron-hole pair could inhibit the degradation process [21]. In spite of all the work devoted to solve these problems, the photocatalytic activity of TiO_2 using visible light has remained quite low, and more work is needed to address this issue. In particular, incorporation of Sn into the TiO_2 has been reported as the most facile doping of TiO_2. It has been reported elsewhere [22–26] that incorporation of some metals can induce crystallization in amorphous materials on annealing at relatively low temperatures. This process, known as metal-induced crystallization [22], has been applied for significant reduction of the solid-phase crystallization temperature of titanium dioxide [23–25]. Particularly, the effect of different cations on the anatase–rutile phase transition temperature, attributed to the atomic mobility enhanced by the empty spaces left by the oxygen deficiency sites occupied by the atoms introduced into the TiO_2 matrix [26]. This seems to be a plausible explanation in the case of Sn. Additionally, the surfactant assisted technique becomes a facile and simple method suitable to obtain Sn-modified TiO_2 with small crystallite size and capable to induce the crystalline transition from anatase to rutile phase at low temperatures, producing mixtures of these phases varying the anatase to rutile ratio, as a function of the Sn content. In this way, to our best knowledge, a novel strategy to control the anatase to rutile ratio using low amounts of Sn and a low temperature procedure for varying the anatase to rutile ratio has been successfully developed. Therefore, the aim of the present work was to investigate the modification of titanium dioxide by introducing different amounts of Sn to the TiO_2 lattice in presence of the P123 surfactant as well as the characterization of the physical properties of the obtained materials. The photocatalytic activity under visible irradiation was determined in the degradation of some NSAIDs, specifically, diclofenac, ibuprofen and paracetamol, present separately and at different concentrations in real wastewaters from a pharmaceutical industry in the State of Mexico.

2. Experimental procedure

2.1. Synthesis of the Sn-modified TiO_2 photocatalysts

The chemical synthesis was carried out using the co-polymer block (Poly(ethylene glycol)-block-poly(propylene glycol)-block-poly(ethylene glycol)) Pluronic P123 from Aldrich, Tin(IV) chloride pentahydrate ($SnCl_4{\cdot}5H_2O$ Purity $\geqslant$ 98%, Aldrich), Titanium isopropoxide ($Ti\{OCH(CH_3)_2\}_4$, Aldrich, 98% purity) and ammonium hydroxide (NH_4OH, Merck, ACS reagent) as reactants. The Sn-modified TiO_2 photocatalysts were synthesized by mixing 8 g of P123 surfactant with 25 ml of 2 M HCl solution; the mixture was vigorously stirred until complete dissolution, followed by a maturing time of 2 h to preform the surfactant template. Afterwards, to obtain catalysts with 0, 5, 10 and 25 wt.% as SnO_2, different quantities of titanium isopropoxide (14.2, 13.5, 12.8 and 10.7 g) and stannic chloride (0, 0.4, 0.9 and 2.3 g) were added and stirred at 60 °C to obtain a homogeneous mixture, which was aged at 60 °C for 24 h under hydrostatic pressure until a white gel was formed; some drops of NH_4OH were added to stabilize the pH of the hydroxylated gel at 5.0. This gel was filtered in vacuum, washed with distilled water to remove the HCl, NH_4OH and chloride ions remaining, then the gel was dried at 50 °C for 12 h. The obtained powders were subjected to thermal treatment at 350 °C in air for 4 h, using a temperature rate of 5 °C/min, with the purpose of eliminate the surfactant and to obtain the photocatalysts as a crystalline material. The different photocatalyst obtained are named TiO_2-Sn(x) hereinafter, where x = 0, 5, 10 and 25 wt.% as SnO_2. The commercial TiO_2 Degussa P25 catalyst was used as a reference.

2.2. Characterization of photocatalysts

The synthesized powders were characterized using the following techniques: (a) Thermogravimetric Analysis and Differential Scanning Calorimetry (TGA/DSC) to determine the temperature of thermal treatment to eliminate the Pluronic P123 surfactant and to obtain crystalline materials. Analysis were taken in a Netzsch equipment, STA 449 F3, Júpiter; with N_2 gas flow (20 ml/min), from environmental temperature up to 1000 °C, heating rate of 3 °C/min. (b) Textural properties were measured by N_2 physisorption technique using an ASAP 2020 equipment from Micromeritics. The surface area was calculated using the Brunauer-Emmett-Teller

(BET) equation, whilst adsorption isotherms were used to determine pore size distributions and the shape of the pores; mean pore diameter was calculated by using the Barrett-Joyner-Halenda (BJH) equation. The total pore volume was determined at relative pressure (P/P^o) equal to 0.98. All samples were degassed out at 250 °C for 3 h (5 μm Hg) prior to N_2 physisorption measurements. (c) surface morphology by Scanning electron microscopy (SEM) (d) Raman spectroscopy (RS) was used to study the microstructure of the powders;spectra were acquired using an HR LabRam 800 system equipped with an Olympus BX-40 confocal microscope; a Nd:YAG laser beam (532 nm) was focused by a 50 X objective onto the sample surface (≈1 μm diameter spot). (e) The crystalline structure of the obtained powders was determined by X-ray powder diffraction (XRD) with a Bruker D8 Advance Diffractometer using the Cu-Kα radiation line (λ = 1.54 Å); the diffraction patterns were recorded in the 2θ interval from 20° to 70° in steps of 0.05°. (f) Elemental chemical composition as well as the chemical state of the elements present in the different samples, were determined by X-ray Photoelectron Spectroscopy (XPS) with a JEOL JPS 9200 equipment using a Mg-Kα X-ray source (1253.6 eV), 200 W and 1×10^{-6} bar of pressure in the analysis chamber, wide and narrow spectra were acquired. (g) Diffuse Reflectance Spectroscopy (DRS) measurements were carried out on a Perkin Elmer Lambda 35 spectrophotometer with the integration sphere; from the DRS spectra the band gap energy was estimated using the Kubelka-Munk method.

2.3. Photocatalytic performance

In order to evaluate the photocatalytic performance of the prepared photocatalysts, real wastewaters from effluents of a pharmaceutical industry in the State of Mexico, containing separately diclofenac, paracetamol and ibuprofen, were treated. This was done with the purpose of evaluate the photocatalytic performance using real wastewaters, containing chlorides, fluorides, phosphates, etc. as was revealed by the physico-chemical characterization performed prior to the photocatalytic experiments. The presence of some of these components could inhibit the degradation of the drugs and even cause the partial or total deactivation of the catalysts. The degradation of each drug was followed by the decrease in its characteristic absorption band, located at 275 nm for diclofenac, 243 nm for paracetamol and 222 nm for ibuprofen, taking aliquots every 15 min during the reaction time (180 min). The absorption spectra of the pharmaceutical solutions were recorded in a Perkin Elmer Lambda 35 spectrophotometer in the absorbance mode. The reaction system, in the batch mode, was prepared by introducing 5 mg of catalyst powder into 25 ml of each pharmaceutical wastewater; afterwards, the solution was stirred in dark conditions in order to reach the adsorption equilibrium between each drug and the catalyst. The powders were activated by illuminating them with a visible light source using an Hg lamp; the spectral emission of the used lamp was characterized by optical emission spectroscopy. It was found an intense line emission at 404 nm and lines of less intensity (<30%) at 435, 365 and 311 nm; keeping the distance between the liquid surface and the light source at 15 cm. The commercial TiO_2 Degussa P25 catalyst was used as a reference sample. A non-linear least square data treatment was used to determine the kinetic rate constant considering a pseudo-first order kinetic model.

3. Results and discussion

3.1. Characterization of TiO_2-Sn(x) photocatalysts

Thermal analysis graph corresponding to the TiO_2-Sn (25) sample (Fig. 1) shows a loss of weight from 0 to 200 °C attributed to the loss of water. A second loss of weight was seen from 200 to 300 °C due to P123 organic compound elimination and finally at approximately 300 °C, the dehydroxylation was observed. It is important to remark that the increase in the Sn content promotes a decrease in the dehydroxylation temperature, from 350 to 300 °C (figures are not shown). From this data the thermal treatment suitable for the total organic compound elimination and dehydroxylation of the photocatalysts was chosen as 350 °C. In order to corroborate the Pluronic P123 surfactant elimination after thermal treatment infrared spectra of materials were recorded. The Pluronic P123 organic compound is characterized by IR features located at 1000–1250, 2690–2840 and 3200–3550 cm^{-1}, corresponding to the C—H, H—O and C—C bonds, respectively [27]. These signals were clearly observed before the thermal treatment of the samples as is observed in Fig. 2. The signal at 1640 cm^{-1} is attributed to the H—O—H molecular water bending mode. From Fig. 2 it is clearly observed that signals corresponding to the Pluronic P123 compound are absent in the IR spectra of the sample after the thermal treatment confirming its elimination.

With the purpose of obtaining information about the surface composition and chemical state of the elements present in the different TiO_2-Sn(x) photocatalysts, the samples were characterized by XPS. Fig. 3 shows the XPS high-resolution spectra of the binding energy regions of: (a) Ti-2p, (b) O-1s and (c) Sn-3d, corresponding to samples with different Sn content. The XPS Ti-2p region show two signals in a doublet peaking at 458.7 and 464.6 eV attributed to Ti-2p3/2 and Ti-2p1/2 respectively (Fig. 3a) related to the anatase phase of the TiO_2 [28]. To perform a deeper analysis, the Ti-2p region of the TiO_2-Sn (25) sample was deconvoluted. Fig. 3d) shows two doublets, the first one located at 458.7 and 464.6 eV and the second one located at 458.5 and 463.7 eV, these doublets attributed to Ti-2p3/2 and Ti-2p1/2 are characteristics of the TiO_2 in its anatase and rutile phases, respectively. This result suggests that Sn incorporation into the TiO_2 lattice promotes the transformation from anatase to rutile. The peak at 530 eV (Fig. 3b) corresponding to O-1s of TiO_2 reveal that the oxygen atoms are bonded with titanium forming TiO_2. The peaks located at 486.3 and 494.7 eV (Fig. 3c) are due to Sn-3d5/2 and Sn-3d3/2 respectively, that could be attributed to Sn in good agreement with the values for the tin in SnO_2 [29]. Table 1 gives the composition data of the prepared catalysts calculated by XPS. It was observed that the prepared catalysts contain 0.0, 2.4, 5.1 and 7.2 at.% of Sn. It is observed that the O/Ti ratio is higher than the stoichiometric ratio for the TiO_2 sample, evidence that an excess in the amount of oxygen exist in the samples. As the Sn content increases the O/Ti ratio

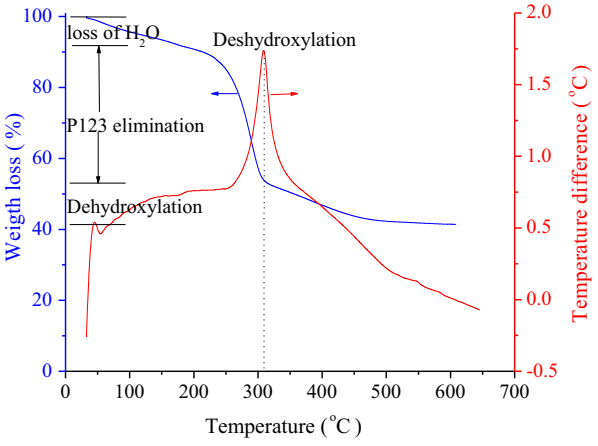

Fig. 1. Thermogravimetric analysis and differential temperature analysis (TGA-DTA) for the TiO_2-Sn(25) catalyst.

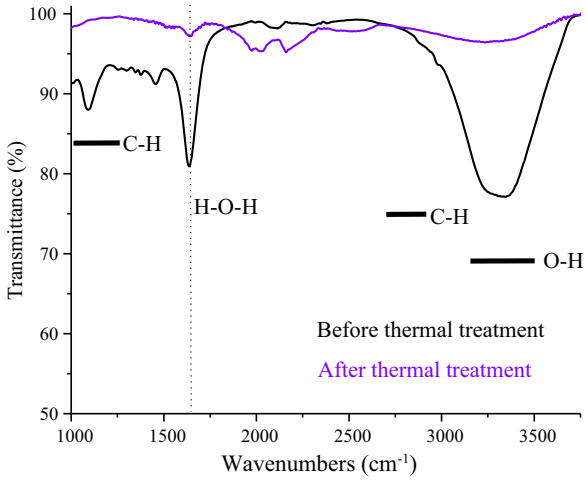

Fig. 2. Infrared spectra of the TiO_2-Sn(25) catalyst before and after the thermal treatment.

increases to higher values whereas the oxygen content remains almost constant. Additionally, for samples containing Sn, the total amount of Sn and Ti is the same; these results suggest that Sn could be occupying Ti sites in the TiO_2 lattice.

Textural properties of the TiO_2-Sn(x) catalysts are presented in Table 2. In general terms, the results indicate that the textural properties are preserved almost the same as in the TiO_2 powders, regardless of the amount of Sn incorporated into the sample. The specific surface area is maintained whereas the mean pore diameter increases by about 20% and the distribution of pore sizes becomes wider, as more Sn is added. This properties were evaluated in order to quantify the exposed area accessible to the wastewater, taking into account that in the photodegradation process only the holes, formed as a result of the interaction photon-semiconductor, that reach the surface are useful for the oxidation of water and consequently for the generation of active species, hydroxyl radicals, responsible of organic molecules degradation. The morphology of the samples was examined using a scanning electron microscopy (SEM) Fig. 4a–d), It can be found that the as-prepared product is composed of agglomerated particles constituted of the crystalline material. The Raman spectra of samples show peaks at 141, 195, 395, 514 and 636 cm^{-1} (Fig. 5a), which are characteristic of the TiO_2 anatase phase [30,31]; additionally, small features at 444 and 609 cm^{-1}, attributed unambiguously to the rutile phase of TiO_2, can also be seen [30,31]. As the atomic content of Sn increased in the TiO_2-Sn(x) powders, two main changes could be observed. First, Fig. 5a clearly shows that as the Sn content increases the peak at 141 cm^{-1} becomes broader and less intense; these changes suggest that the Sn atoms are distorting the Ti-O-Ti lattice, inducing structural disorder. Second, a closer view of the Raman spectra (Fig. 5b), reveals that as more Sn is added, the peaks associated with the rutile phase (444 and 609 cm^{-1}) increase their intensity showing clearly the phase transition from anatase to rutile; this results suggest that Sn incorporation into the anatase lattice favors the phase transition to rutile at temperatures as low as 350 °C, which is in good agreement with previous reports [25,29,32]. It is worth noting that no signals associated with SnO_2 in its cassiterite crystalline phase were observed probably due to a dilution effect and to the fact that the main peak of this oxide appears at 638 cm^{-1}, very close to the TiO_2 anatase Raman peak. The absence of the SnO_2 Raman signal, could indicate that Sn is introduced into the TiO_2 lattice forming a solid solution crystallizing in the TiO_2 rutile phase.

Fig. 6 shows the XRD patterns of the samples with different tin contents. The pattern corresponding to the TiO_2 powder without

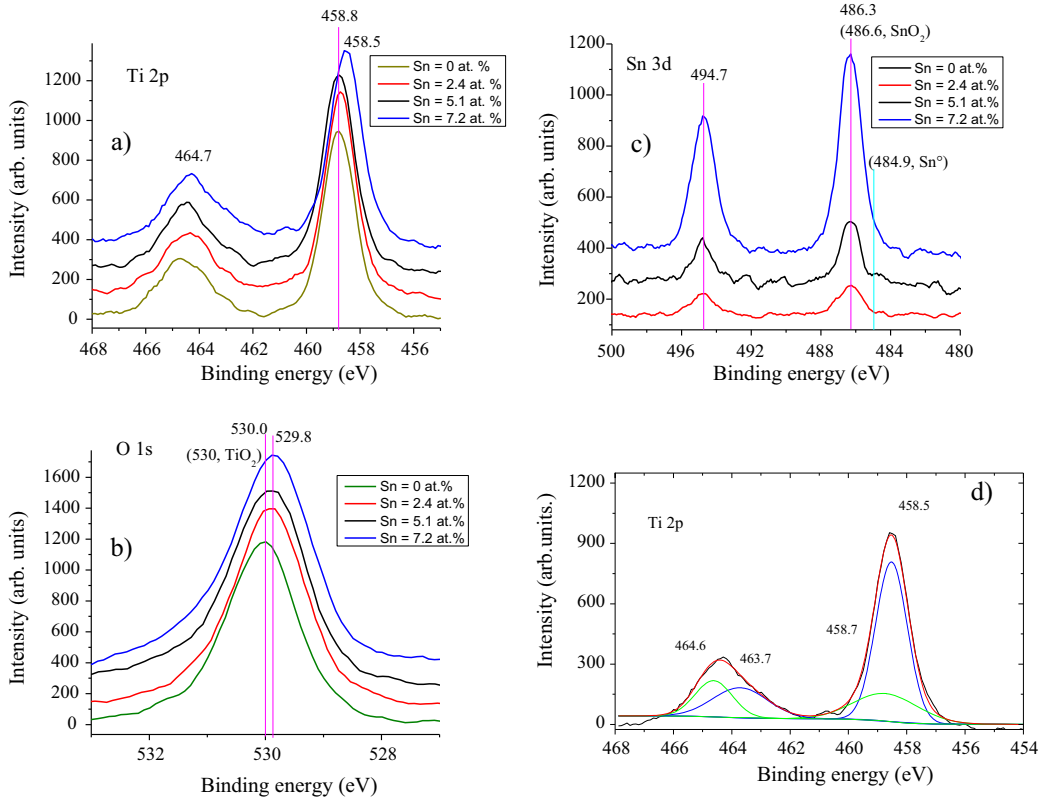

Fig. 3. XPS spectra of (a) Ti 2P region, (b) O 1s region, (c) Sn 3d region and (d) deconvoluted Ti 2P region for TiO_2-Sn(25) catalyst.

Table 1
Elemental composition.

Catalyst	Elemental content (at.%)			O/Ti ratio
	Ti	Sn	O	
TiO_2-Sn(0)	29.8	0.0	70.2	2.3
TiO_2-Sn(5)	26.4	2.4	71.2	2.7
TiO_2-Sn(10)	23.7	5.1	71.2	3.0
TiO_2-Sn(25)	21.0	7.2	71.9	3.4

Table 2
Textural properties of TiO_2-Sn(x) catalysts.

Catalyst	Mean pore diameter (Å)	Pore volume (cm^3/g)	Surface área (m^2/g)
TiO_2-Sn(0)	99	0.3	105
TiO_2-Sn(5)	123	0.4	82
TiO_2-Sn(10)	120	0.4	109
TiO_2-Sn(25)	126	0.4	107

Sn show peaks at $2\theta = 25.3°$, 36.1°, 48.1°, 54.4°, 56.5° and 62.7°, characteristics of the anatase phase of titanium dioxide (JCPDS card73-1764). It is clearly observed that this phase remains for the different contents of tin in good agreement with the XPS and Raman results. Additionally, peaks at $2\theta = 27.4°$, 35.9°, 41.1° and 54.2°, corresponding to the rutile phase (JCPDS 75-1753), are also present. Therefore, the XRD results reveal a mixture of the TiO_2 crystalline phases, anatase and rutile, present in the different samples. It is observed that as the Sn content increases, the intensity of the rutile pattern lines increase, with respect to the anatase lines, indicating a greater crystallite amount of the rutile phase [33]. Rietveld refinement analysis was performed to complement the XRD study, determining the crystallite size and the proportion of each crystalline phase; the results are presented in Table 3. According to the Rietveld refinement, the proportion of the anatase crystalline phase decreases as the Sn content increases, from 62.9% in pure TiO_2 to 4.0% for a Sn content of 7.2 at.%. On the other hand, the amount of the rutile phase increases from 37.1% in pure titania to 96.0% in the sample modified with the highest Sn content. The mean crystallite size for anatase was between 8.5 and 10.5 nm, whereas the size of the rutile crystals diminished from 16.5 to 4.4 nm as the content of Sn was increased, suggesting that tin inhibits the rutile crystal growth. These results are consistent with the Raman characterization, revealing that the obtained powders are composed of a mixture of crystalline phases in different proportions in which some of Sn atoms are occupying sites in the TiO_2 lattice. Additionally, it must be pointed out that no signals attributed to the SnO_2 crystalline phase were observed by XRD in good agreement with the Raman results.

Table 4 includes, the optical band gap (Eg) values determined using the Kubelka-Munk method; this was done by transforming the reflectance spectra of the catalysts with different Sn contents to the Kubelka-Munk function, F(R), and then plotting $(F(R)\,E)^{1/2}$ versus E. The Eg values were obtained by a linear fit of the linear portions of the curve, determining its intersection with the photon energy axis [34]. In these cases, the employed method allows the determination of the band gap values with good accuracy for the TiO_2-Sn(0) and the TiO_2-Sn(5); however, it was not possible to perform the fitting of the spectra corresponding to the TiO_2-Sn(10) and TiO_2-Sn(25) catalysts. As is observed in Table 3, the obtained results reveal that when Sn is incorporated in the photocatalysts, the band gap narrows from 2.8 eV ($\lambda = 442$ nm) to values as low as 2.6 eV ($\lambda = 477$ nm), remarking that the low bandgap values of the prepared catalysts allow their activation with the visible light source employed in this case (404 nm).

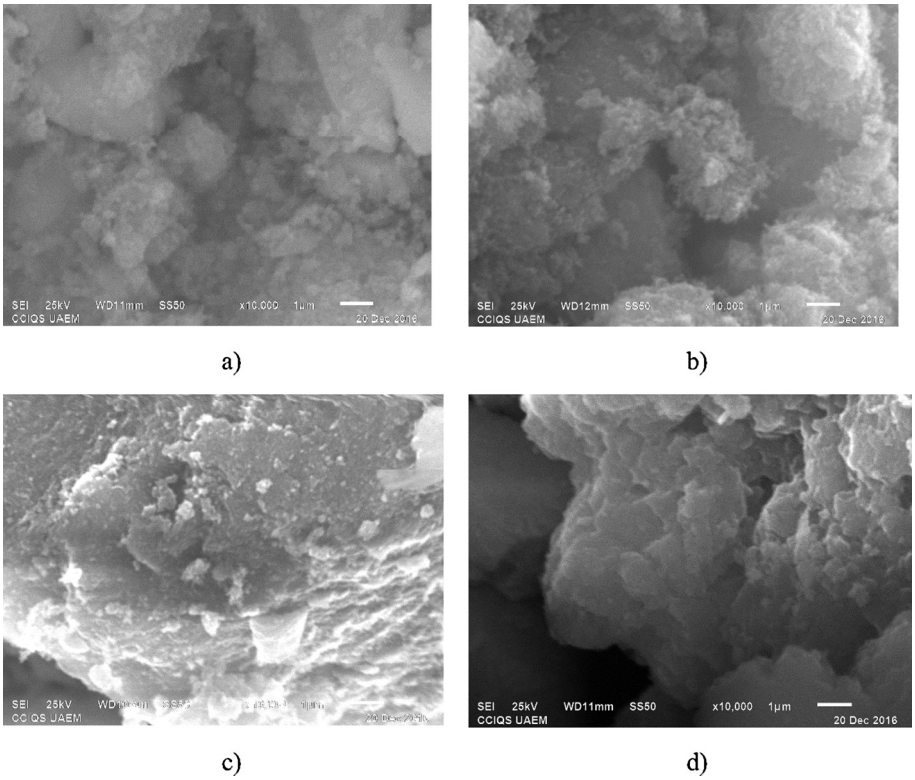

Fig. 4. Scanning electron microscopies of TiO_2-Sn(x) photocatalysts, x = (a) 0, (b) 5, (c) 10 and (d) 25 wt.% of SnO_2.

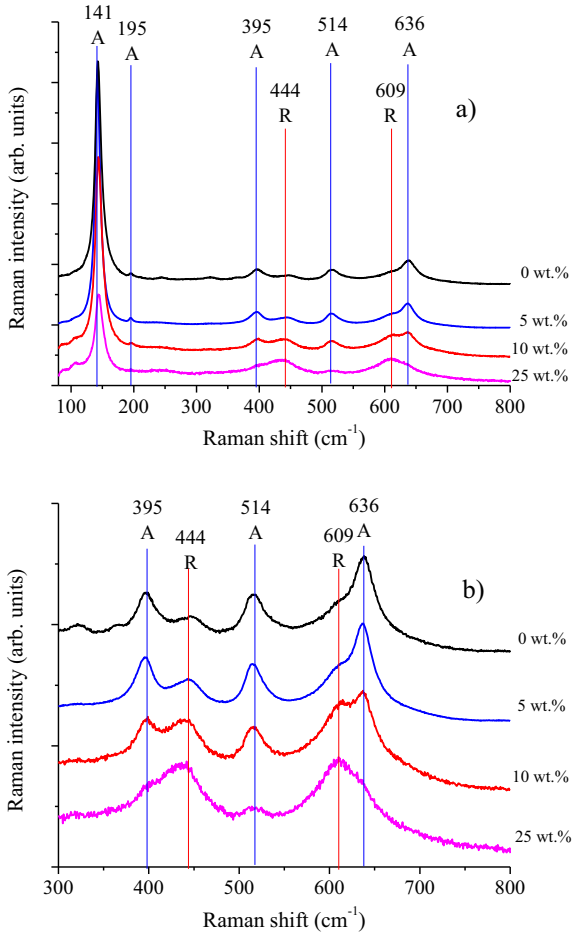

Fig. 5. Raman spectra for the TiO_2-Sn(x) catalysts.

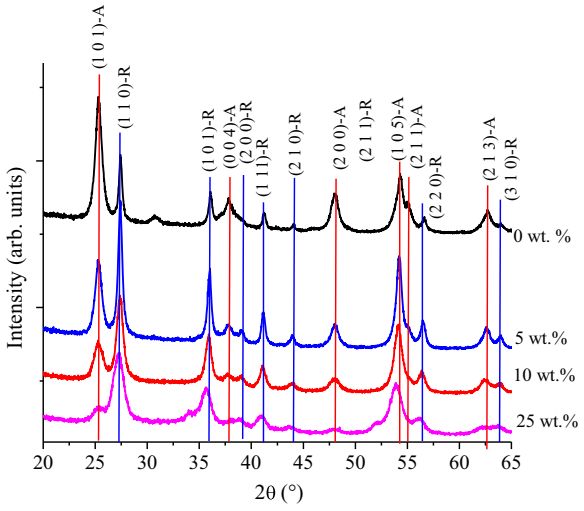

Fig. 6. X-ray powder diffraction patterns of the different TiO_2-Sn(x) catalysts.

3.2. Photocatalytic performance of TiO_2-Sn(x) catalysts in degradation of drugs contained in pharmaceutical wastewaters

The photocatalytic performance of each TiO_2-Sn(x) catalyst was tested in the degradation of NSAIDs, diclofenac, ibuprofen and paracetamol, present separately in real wastewaters, obtained from three different streams, from a pharmaceutical industry of the State of Mexico. Prior to the tests, wastewaters were characterized by the parameters listed in Table 5. The initial concentrations of the NSAIDs were: (a) diclofenac, 3.57 ± 0.06 mg/l, (b) paracetamol, 194.51 ± 0.04 mg/l and (c) ibuprofen, 2.82 ± 0.07 mg/l. It is important to note that paracetamol is present in a higher concentration (~50 times) than the diclofenac and ibuprofen. The photodegradation degree for each molecule was determined by following their characteristic UV–Vis absorption bands located at: (a) 275 nm for diclofenac, (b) 243 nm for paracetamol and (c) 222 nm for ibuprofen. Fig. 7 shows the results obtained for the degradation of the NSAIDs tested, after 180 min of reaction. The data for the photodegradation using the commercial Degussa P25 catalyst is included for comparison purposes. Table 4 shows the reaction rate constant values k_{app} (min^{-1}) was obtained from fitted concentration through reaction time assuming a pseudo first-order expression (exponential curve) using a non linear least square data treatment with an acceptable precision [35]; this values are in accordance with the photocatalytic degradation degree reached for each photocatalyst evaluated. Photodegradation of diclofenac shows a maximum degradation degree, close to 25% after 180 min, using the TiO_2-Sn(0) catalyst. As the Sn was added and its content increases in the catalytic formulation, the degradation degree decreases monotonically to values around 20%, 12% and 10% for Sn contents of 2.4, 5.1 and 7.2 at.% respectively. The results for paracetamol degradation show a very similar behavior, as the Sn content increases the maximum degradation decreases, but with values lower than diclofenac; in this case the sample TiO_2-Sn(0) reaches the highest degradation degree, close to 18%, whereas the sample TiO_2-Sn(10) exhibited the lowest degradation degree suggesting that formulations containing Sn are not the best option to degrade paracetamol. However, it is important to point out that the concentration of paracetamol was almost 50 times greater than the concentration of diclofenac and concentration has a very strong effect on the photocatalytic response. In contrast to the paracetamol and diclofenac degradation, the ibuprofen drug was degraded more efficiently as the Sn content increased, except for the sample with the highest content of Sn. The TiO_2-Sn(10) photocatalysts reached the highest degradation degree close to 25% as is shown in Fig. 7, while the catalyst without Sn reached only 17% of degradation. Concerning the results obtained using the commercial catalyst Degussa P25, for diclofenac and ibuprofen lower degradation degrees were obtained. In the case of diclofenac, the prepared photocatalyst were more than 3 times better, whereas for ibuprofen almost 2 times better. In the case of paracetamol, the commercial catalyst (Degussa P25) showed an activity very close to the obtained with the TiO_2-Sn(0) catalyst and higher compared with the catalysts containing Sn. Three aspects must be emphasized from the obtained results: first, it is important to remark that the highest catalytic conversion reached for each of these pharmaceutical drugs was very low, between 16 and 25%, for all the photocatalysts including Degussa P25, demonstrating that in some cases the prepared catalysts are better than the commercial one. These low activities can be attributed to some factors: (a) the physicochemical characteristics of the real wastewaters used that contain suspended solids, chlorides, fluorides, sodium hypochlorite, etc. that contribute to the turbidity of the wastewaters diminishing consequently the light intensity that reaches the catalyst surface; (b) the high initial concentration of each drug tested, particularly in the case of paracetamol, approximately two orders of magnitude greater than diclofenac, this can also contribute to increase the water turbidity; (c) the presence of contaminants in the water such as chlorides which can deactivate the catalysts by poisoning. Second, it is clearly observed in Fig. 7, that each NSAIDs was degraded at different rate depending on the photocatalyst employed, ibuprofen is degraded more efficiently by the TiO_2-Sn(10) catalyst while for diclofenac degradation the TiO_2-Sn

Table 3
Proportion of crystalline phases and mean crystallite size from Rietveld refinement.

	Proportion of crystalline phases		Anatase:Rutile ratio	Mean crystallite size (nm)	
Catalyst	Rutile (%)	Anatase (%)		Rutile (nm)	Anatase (nm)
TiO_2-Sn(0)	37.1	62.9	1.69	16.5	8.5
TiO_2-Sn(5)	64.9	35.1	0.54	13.4	8.5
TiO_2-Sn(10)	76.3	23.7	0.31	8.3	6.9
TiO_2-Sn(25)	96.0	4.0	0.04	4.4	10.5

Table 4
Band gap energy (eV) and kinetic rate constant (k_{app}) as a function of Sn content.

Photocatalyst	Band gap energy (eV)	k_{app} (min^{-1}) ibuprofen	k_{app} (min^{-1}) paracetamol	k_{app} (min^{-1}) diclofenac
TiO_2-Sn(0)	2.8	0.0034 ± 5 E−5	0.0024 ± 4 E−5	0.0128 ± 5 E−5
TiO_2-Sn(5)	2.6	0.0061 ± 2 E−5	0.0012 ± 7 E−5	0.0069 ± 6 E−5
TiO_2-Sn(10)	n.d.	0.0172 ± 8 E−5	0.0009 ± 9 E−5	0.0013 ± 8 E−5
TiO_2-Sn(25)	n.d.	0.0093 ± 3 E−5	0.0010 ± 6 E−5	0.0011 ± 7 E−5

Table 5
Physicochemical characterization of wastewater.

Physicochemical characteristics	
Temperature (°C)	15.6
Dissolved oxygen (mg/l)	12.2
Conductivity (μS/cm^{-1})	143.2
pH	6.3
Chlorides (mg/l)	101.0
Fluorides (mg/l)	3.8
Hardness (mg/l)	245.7
Ammonium (mg/l)	0.73
Total suspended solids (mg/l)	36.0
Total phosphorous (mg/l)	73.0
Total nitrogen (mg/l)	18.0
Biochemical oxygen demand (BOD) (mg/l)	33.0
Sodium hypochlorite (mg/l)	1.0

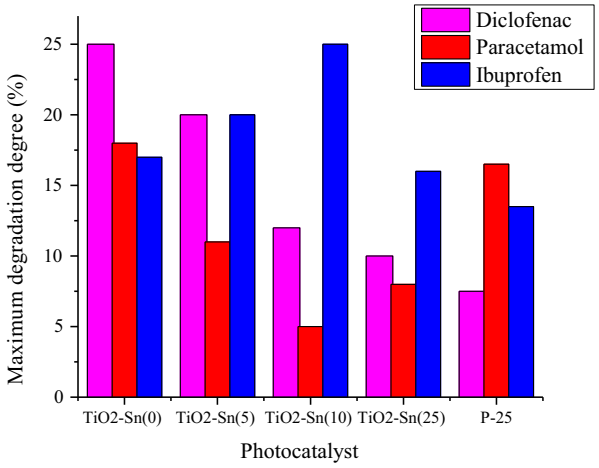

Fig. 7. Photocatalytic performance after 180 min of reaction time under visible light.

(0) photocatalyst shows the highest degradation degree. Paracetamol was degraded almost equally by the TiO_2-Sn(0) and the Degussa P25; these results seem to indicate a certain kind of selectivity or affinity of each catalyst with a specific drug, TiO_2-Sn(10) catalyst with ibuprofen, TiO_2-Sn(0) with diclofenac and TiO_2-Sn (0) with paracetamol. Third, it is important to consider that the samples are composed by different mixtures of the anatase/rutile crystalline phases due to the Sn incorporation into the TiO_2 lattice, which could result in lower band gap values as well as the coupling of these two semiconductors making the correlation of the physical properties with the catalytic formulations a multifactorial problem. Additional work is underway in order to gain insight about these issues.

4. Conclusions

It was found that the employed synthesis procedure promotes the formation of a mixture of the anatase/rutile phases with the development of the TiO_2 rutile phase at temperatures as low as 350 °C. The addition and increase of the Sn amount to the TiO_2-Sn(x) catalytic formulations increases the proportion of the rutile phase allowing to tailor the anatase to rutile ratio. The role of Sn into the TiO_2 lattice is to promote the anatase to rutile phase transition at low temperature. It was found that the photocatalytic performance depends on the anatase to rutile ratio and in spite of the low degradation obtained, the prepared materials are better than the P25 commercial catalyst, being potentially useful and suitable to degrade NSAIDs present in real wastewaters using visible light. Another important fact that deserves to be mentioned is that the synthesized powder TiO_2-Sn(x) photocatalysts can be removed from the reaction system in an easier way than the small particle size Degussa P25 analog.

Acknowledgements

The authors thank UAEM for the financial support through the project 3458 CHT. Thanks also to the staff of the SIEA-UAEM for their help and technical support. This work was partially supported by CONACYT, under the project CB-168827. D. Solis thanks to Lizbeth Triana, Alejandra Nuñez, Uvaldo Balderas, Melina Tapia and Citlalit Martinez for the technical assistance.

References

[1] Chonova T, Keck F, Labanowski J, Montuelle B, Rimet F, Bouchez A. Separate treatment of hospital and urban wastewaters: a real scale comparison of effluents and their effect on microbial communities. Sci Total Environ 2016;542:965–75.
[2] Aguilar CP, Peruzzolo M, Di Luccio M, Dallago RM, Filho IDN. Qualitative study of organic compounds in wastewaters of a swine slaughterhouse. Environ Monit Assess 2006;116(1–3):103–10.
[3] Parolini M, Binelli A. Sub-lethal effects induced by a mixture of three non-steroidal anti-inflammatory drugs (NSAIDs) on the freshwater bivalve Dreissena polymorpha. Ecotoxicol 2012;21:379–92.
[4] Simon JP, Prince SE. Natural remedies for non-steroidal anti-inflammatory drug-induced toxicity. J Appl Toxicol 2017;37:71–83.
[5] Memmert U, Peither A, Burri R, Weber K, Schmidt T, Sumpter JP, et al. Diclofenac: new data on chronic toxicity and bioconcentration in fish. Environ Toxicol Chem 2013;32(2):442–52.

[6] Dionysiou DD, Suidan MT, Bekou E. Effect of ionic strength and hydrogen peroxide on the photocatalytic degradation of 4-chlorobenzoic acid in wáter. Appl Catal B 2000;26:153–71.
[7] Pelegrini R, Peralta-Zamora P, de Andrade AR, Reyes J, Nelson Durán. Electrochemically assisted photocatalytic degradation of reactive dyes. Appl Catal B 1999;22:83–90.
[8] Fox MA, Dulay M. Heterogeneous photocatalysis. Chem Rev 1993;93:341–57.
[9] Fujishima A, Zhang X, Tryk DA. TiO_2 photocatalysis and related surface phenomena. Surf Sci Rep 2008;63:515–82.
[10] Ohtani B. Photocatalysis A to Z—What we know and what we do not know in a scientific sense. J Photochem Photobiol C: Photochem Rev 2010;11:157–78.
[11] Henderson MA. A surface science perspective on TiO_2 photocatalysis. Surf Sci Rep 2011;66:185–297.
[12] Lettmann C, Hinrichs H, Maier WF. Combinatorial discovery of new photocatalysts for water purification with visible light. Angew Chem Int Ed 2001;40(17):3160–4.
[13] Bahnemann D. Photocatalytic water treatment: solar energy applications. Sol Energy 2004;77:445–59.
[14] Lorret O, Francova D, Waldner G, Stelzer N. W-doped titania nanoparticles for UV and visible-light photocatalytic reactions. Appl Catal B: Environ 2009;91:39–46.
[15] Lin J, Yu JC, Lo D, Lam SK. Photocatalytic activity of rutile $Ti_{1-x}Sn_xO_2$ solid solutions. J Catal 1999;183:368–72.
[16] Karthikeyan N, Narayanan V, Stephen A. Degradation of textile effluent using nanocomposite TiO_2/SnO_2 semiconductor photocatalysts. Int J Chem Tech Res 2015;8(11):443–9.
[17] Xu L, Steinmiller E, Skrabalak SE. Achieving synergy with a potential photocatalytic Z-scheme: synthesis and evaluation of nitrogen-doped TiO_2/SnO_2 composites. J Phys Chem C 2012;116:871–7.
[18] Camps E, Escobar-Alarcón L, Camacho-López MA, Solis Casados DA. Visible-light photocatalytic activity of nitrided TiO_2 thin films. Mater Sci Eng B 2010;174:80–3.
[19] Khan R, Kim TJ. Preparation and application of visible-light-responsive Ni-doped and SnO_2-coupled TiO_2 nanocomposite photocatalysts. J Hazard Mater 2009;163:1179–84.
[20] Chung-Hsin W. Comparison of azo dye degradation efficiency using UV/single semiconductor and UV/coupled semiconductor systems. Chemosphere 2004;57:601–8.
[21] Malathy M, Vignesh K, Rajarajan M, Suganthi A. Enhanced photocatalytic performance of transition metal doped Bi_2O_3 nanoparticles under visible light irradiation. Ceram Int 2014;40:101–7.
[22] Wang Z, Jeurgens LPH, Mittemeijer EJ. Metal-induced crystallization fundamentals and applications. Singapore: Standford Publishing Pte. Ltd; 2015.
[23] Shuibin Y, Xuehong L, Biao C, Siqun H. The microwave synthesis and photocatalytic activity of SnO_2 TiO_2 nanocomposite. J Wuhan Univ Technol – Mater Sci Ed 2005;20(3):78–80.
[24] Varma LD, Mohiddon MA, Ghanashyam M. Low temperature Au induced crystallization of titanium dioxide thin films for resistive switching applications. RSC Adv 2015;5:67493–9.
[25] Perkas N, Pol GP, Pol SV, Gedanken A. Gold-induced crystallization of SiO_2 and TiO_2 powders. Cryst Growth Des 2006;6(1):293–6.
[26] Vargas S, Arroyo R, Haro E, Rodriguez R. Effects of cationic dopants on the phase transition temperature prepared by the sol-gel method. J Mater Res 1999;14:3932–7.
[27] Liao DL, Liao BQ. Shape, size and photocatalytic activity control of TiO_2 nanoparticles with surfactants. J Photochem Photobiol A: Chem 2007;187(2–3):363–9.
[28] Grunwaldt JD, Göbel U, Baiker A. Preparation and characterization of thin TiO_2-films on gold/mica. J Anal Chem 1997;358:96–100.
[29] Wang W, Niu J, Ao L. Large-scale synthesis of single-crystal rutile SnO_2 nanowires by oxidizing SnO nanoparticles in flux. J Crystal Growth 2008;310:351–5.
[30] Wang WK, Chen JJ, Zhang X, Huang YX, Li W, Yu HQ. Self-induced synthesis of phase junction TiO_2 with a tailored rutile to anatase ratio below phase transition temperature. Sci Rep 2016;6. article 20491.
[31] Ocaña M, Fornés V, García Ramos JV, Serna CJ. Factors affecting the infrared and Raman spectra of rutile powders. J Solid State Chem 1988;75(2):364–72.
[32] Solís-Casados DA, Vigueras-Santiago E, Hernández-López S, Camacho-López MA. Characterization and catalytic performance of tin oxide. Ind Eng Chem Res 2009;48(3):1249–52.
[33] Karunakaran C, SakthiRaadha S, Gomathisankar P. Hot-Injection synthesis of bactericidal Sn-doped TiO_2 nanospheres for visible-light photocatalysis. Mater Express 2012;2(4):319–26.
[34] Bianchi CL, Sacchi B, Piro C, Demartin F, Cerrato G, Morandi S, et al. Aspirin and paracetamol removal using a commercial micro-sized TiO_2 catalyst in deionized and tap water. http://dx.doi.org/10.1007/s11356-016-7781-z.
[35] Lente G. Deterministic kinetics in chemistry and systems biology. The dynamics of complex reaction networks. Springer International Publishing; 2015. p. 52–8.